Frequency-swept pulses for ultrafast spatially encoded NMR

Jean-Nicolas Dumez

Frequency-swept pulses for ultrafast spatially encoded NMR

Jean-Nicolas Dumez

Université de Nantes, CNRS, CEISAM UMR 6230, 44000 Nantes, France

Abstract

Ultrafast NMR based on spatial encoding yields arbitrary multidimensional spectra in a single scan. The dramatic acceleration afforded by spatial parallelisation makes it possible to capture transient species and processes, and has notably been applied to the monitoring of reactions and the analysis of hyperpolarised species. At the heart of ultrafast NMR lies the spatially sequential manipulation of nuclear spins. This is virtually always achieved by combining a swept radio-frequency pulse with a magnetic field gradient pulse. The dynamics of nuclear spins during these pulse sequence elements is key to understand and design ultrafast NMR experiments, and can often be described by surprisingly simple models. This article describes the spatial encoding of relaxation, chemical shift and diffusion in a common framework and discusses directions for future developments.

Keywords: frequency-swept pulses, ultrafast NMR, spatial encoding.

1. Introduction

Swept radio-frequency pulses have found a variety of applications in all areas of magnetic resonance, including nuclear magnetic resonance spectroscopy of liquids and solids, magnetic resonance imaging and electron paramagnetic resonance [1]. Frequency-swept pulses are often used to achieve a rotation of the spins that is less sensitive to the exact calibration of the pulse, or that requires a lower maximum amplitude to cover a given frequency bandwidth. These features are obtained by performing a sequential rather than simultaneous rotation of the spins, in contrast to the case of purely amplitude-modulated selective pulses, that rotate all the selected spins simultaneously.

When a frequency-swept pulse is applied together with a magnetic field gradient pulse, the spectrally sequential rotation also becomes spatially sequential. For a pulse of duration T, the spins rotate at a time $t_{\text{flip}}(z)$ that ranges from 0 to T. This property has been exploited to develop a range of "ultrafast" NMR experiments [2], that map the otherwise incremented indirect dimension of a multidimensional NMR experiment onto a spatial dimension. The indirect dimensions that have been parallelised in this way include the incremented relaxation delay of inversion-recovery experiments [3], the incremented gradient area of diffusion-ordered spectroscopy experiments [4], and the incremented evolution delay of 2D NMR experiments [5, 6, 7]. These correspond to spatial encoding of the longitudinal relaxation time, of the translational diffusion coefficient, and of the chemical shift.

Spatial encoding makes it possible to accelerate the acquisition of multidimensional NMR data by several orders of magnitude, down to a single scan [2]. The resulting ultrafast NMR pulse sequences have been used for a range of applications that include the monitoring of chemical and biochemical reactions [8, 9, 10, 11, 12, 13], the analysis of hyperpolarised substrates [14, 15, 16], and quantitative 2D NMR metabolomics [17, 18]. Spatial encoding, of chemical shifts, is also present in filters to suppress zero-quantum coherences [19], and in the pure-shift yielded by chirp excitation (PSYCHE) method [20]. These applications all rely on pulse sequence developments.

In this article, the spin dynamics during frequency-swept pulses that are relevant to spatial encoding experiments are described. Using numerical simulation and analytical descriptions, a unified description is given of spatial encoding of relaxation, chemical shifts and diffusion. The resulting tools could benefit to the understanding of existing ultrafast NMR experiments, and the design of new or improved experiments.

2. Concept

Figure 1 shows a schematic representation of the position-dependent magnetisation of a an ensemble of uncoupled spins, for spatial encoding of relaxation, chemical shifts and diffusion. In Fig. 1a, the magnitude of the magnetisation reflects the progressive recovery as a function of the recovery delay. In Fig. 1b, the phase of the magnetisation reflects the precession as a function of the evolution delay. In Fig. 1c, the magnitude of the magnetisation reflects the progressive attenuation as a function of the gradient area.

The case of relaxation spatial encoding is perhaps the simplest to understand [3, 11, 21]. The concept was borrowed from an earlier work by Pipe, for MRI applications [22], and the corresponding pulse sequence element is shown in Fig. 2a. It achieves spatial parallelisation of the inversion-recovery experiment. The magnetisation is initially at equilibrium, and a 180° linearly frequency-swept pulse, called a chirp pulse, of duration T_e, is applied together with a magnetic field gradient pulse

Email address: jean-nicolas.dumez@univ-nantes.fr (Jean-Nicolas Dumez)

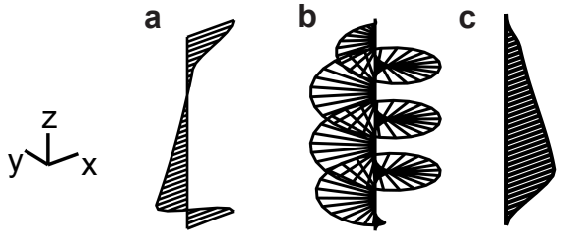

Figure 1: Spatial encoding of (a) relaxation rate, (b) chemical shift, and (c) diffusion coefficient, for an ensemble of uncoupled spins. The transverse magnetisation is shown as a function of position along the z axis. In (a), the relaxation rate is encoded in the position-dependent amplitude. In (b), the spin chemical shift is encoded in the position-dependent phase. In (c), the diffusion coefficient is encoded in the position dependent amplitude. In the three cases, the spatial profile also reflects the time-envelope of the frequency-swept pulse used for spatial encoding.

to sweep over a region of length L_s. The chirp pulse is followed by a hard 90° pulse. As a result, the recovery delay for spins of position z is $\tau(z) = T_e - t_{\text{flip}}(z)$ and ranges linearly from 0 at one end of the spatial region to T_e at the other end, which yields the magnetisation pattern shown in Fig. 1a.

The encoding of chemical-shifts and diffusion coefficients can both be achieved by the joint application of a magnetic-field gradient pulse and a chirp pulse, most frequently a 180° pulse. This scheme results in a position-dependent effective precession time $\tau(z) = T_e - 2t_{\text{flip}}(z)$, ranging linearly from T_e at one end of the spatial region to $-T_e$ at the other end. During this delay, nuclear spins precess under the combined effect of the chemical shift and the magnetic-field gradient. As a result, the effective chemical-shift evolution delay and gradient area are mapped onto a spatial dimension and also depend linearly on position. In experiments in which chemical shifts or diffusion coefficients are encoded, a pair of chirp+gradient blocks is used, as shown in Fig. 2b-c with the example of 180° pulses, with delays and gradient signs chosen to preferentially encode diffusion coefficients or chemical shifts, as will be explained in section 6.

Ultrafast NMR pulse sequences combine spatial encoding of NMR parameters together with a fast acquisition scheme that simultaneously provides spatial resolution and another dimension (spectral or relaxation). Several such schemes have been used, mainly echo-planar spectroscopic imaging (EPSI) [2, 23, 11], and CPMG [15], but also the application of a weak readout gradient [4] and the consecutive acquisition of slice selective spectra [3]. These schemes and their features in the context of ultrafast 2D experiments are described, e.g., in Ref. [24], and will not be discussed here.

High-resolution NMR experiments that rely on spatial encoding of NMR parameters were first reported in 2002 by Frydman and coworkers for ultrafast 2D NMR spectroscopy (UF 2D NMR) [2], and in 2003 by Keeler and co-workers for ultrafast inversion recovery (UF IR) and ultrafast diffusion-ordered NMR spectroscopy (UF DOSY) [3, 4]. In the case of UF 2D NMR, a series of discrete selective pulses was originally used, and it was soon superseded by continuous spatial encoding using frequency-swept pulses [5, 6, 7]. While these methods have

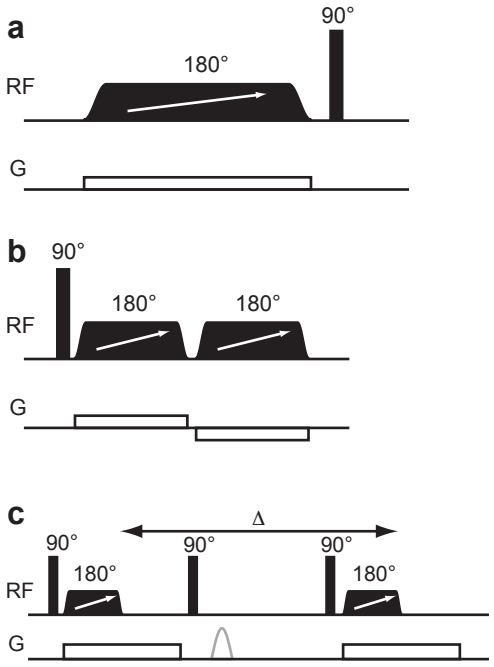

Figure 2: Pulse sequence elements for ultrafast spatially encoded NMR. (a) Ultrafast inversion-recovery experiment. (b) Ultrafast 2D NMR using constant time encoding. (c) Ultrafast diffusion-ordered spectroscopy using a stimulated echo. RF pulses are shown as black rectangles. Frequency-swept pulses are indicated by a white arrow. Gradient pulses for spatial encoding are shown in black. The spoiler gradient for the stimulated echo is shown in grey for UF DOSY. Δ is the diffusion delay. When applied to an initial longitudinal magnetisation, these pulse sequence elements result in the magnetisation patterns shown in Fig. 1. The acquisition blocks of the pulse sequence are not shown.

been reported under different names, we will use the single term ultrafast NMR to refer to them; the initialism UF 2D NMR will refer here only to 2D experiments where the two dimensions are spectral dimensions (chemical shift and/or J couplings). Spatial encoding of diffusion and relaxation has also been exploited in methods that correlate two diffusion or relaxation dimensions, named ultrafast Laplace NMR (UF LNMR) [21, 15].

3. Frequency-swept pulses for spatial encoding

A swept radio-frequency (RF) pulse is characterised by its time-dependent frequency $\omega_{\text{rf}}(t)$ in a rotating frame of reference. The Cartesian components of the RF field are, in that frame:

$$B_{1x} = B_{1\text{max}} A(t) \cos\left(\phi_{\text{rf}}(t) + \phi^0_{\text{rf}}\right), \tag{1}$$

$$B_{1y} = B_{1\text{max}} A(t) \sin\left(\phi_{\text{rf}}(t) + \phi^0_{\text{rf}}\right), \tag{2}$$

where $B_{1\text{max}}$ is the pulse amplitude, $A(t)$ an envelope function, ϕ^0_{rf} a constant phase shift, and

$$\phi_{\text{rf}}(t) = \int_0^t \omega_{\text{rf}}(t')dt', \qquad \text{for} \qquad 0 < t < T_e, \tag{3}$$

where T_e is the duration of the pulse.

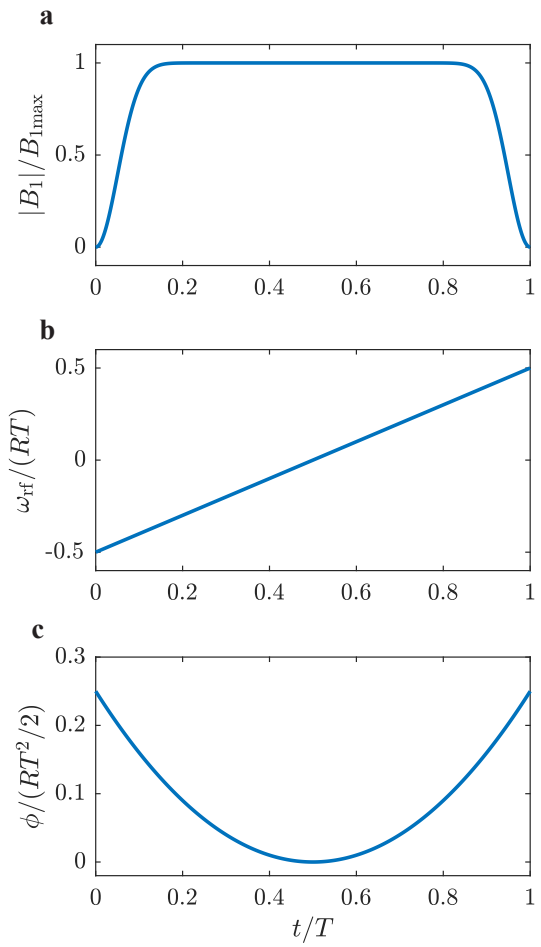

Figure 3: Linearly frequency-swept chirp pulse with a WURST envelope. The amplitude (a), frequency (b) and phase (c) are shown as a function of time.

Virtually all ultrafast NMR experiments rely on linearly-swept, so-called "chirp" pulses. The time-dependent frequency of a chirp pulse is

$$\omega_{\rm rf}(t) = \omega_{\rm rf}^0 + Rt, \tag{4}$$

where R is the sweep rate of the pulse, and $\omega_{\rm rf}^0$ its initial frequency. The time-dependent phase of the pulse is:

$$\phi_{\rm rf}(t) = \int_0^t \omega_{\rm rf}(t')dt' = \omega_{\rm rf}^0 t + \frac{1}{2}Rt^2. \tag{5}$$

Such pulse sweeps over a bandwidth $BW = |R|T_e/(2\pi)$. Several envelope functions have been described for linearly-swept pulses [25, 26]. They are typically constant over the central part of the pulse, with a smooth transition between 0 and 1 at the edges to avoid truncation wiggles in the selected profile. Figure 3 shows an example of chirp pulse with a WURST envelope [26].

When a chirp pulse is applied in the presence of a magnetic field gradient of intensity G, the frequency sweep also becomes

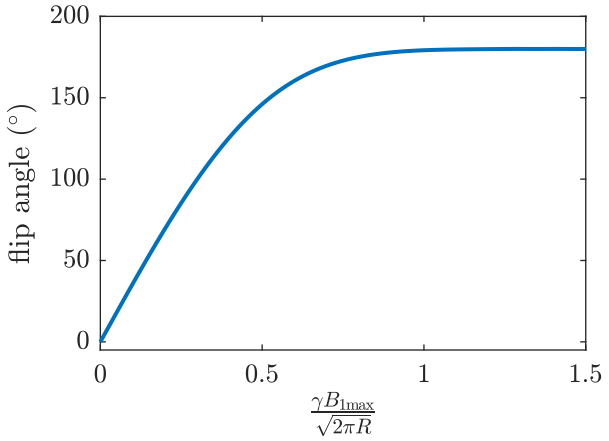

Figure 4: Flip angle experienced by the magnetisation after the application of a chirp of sweep rate R, as a function of the pulse amplitude.

a spatial sweep, over a region of length

$$L_s = \frac{RT_e}{\gamma G}, \tag{6}$$

where γ is the gyromagnetic ratio. This spatial sweep is the central ingredient of ultrafast NMR experiments.

Figure 4 shows the flip angle as a function of the pulse amplitude for a chirp pulse of sweep rate R. Frequency-swept pulses are most frequently used to achieve a 180° rotation of the spins. Above some threshold, in the adiabatic regime, a rotation of 180° is achieved irrespective of the pulse amplitude. The adiabaticity factor of a chirp pulse is $Q = \gamma^2 B_{1\max}^2/R$, and values of Q larger than 5 are typically used for adiabatic 180° pulses. Chirp pulses can also be used to achieve a rotation by an arbitrary angle $\theta < 180°$. For low values of the pulse amplitude, the flip angle varies linearly with the pulse amplitude. Specifically, a pulse amplitude of $B_{1\max} \simeq 0.26\sqrt{2\pi R}/\gamma$ ($Q \simeq 0.44$) results in a flip angle of 90° [27]. A very good approximation for θ as a function of Q has been derived [28]:

$$\theta = \arccos\left(2\exp(-\pi Q/2) - 1\right). \tag{7}$$

4. Numerical methods

Numerical simulations were used to illustrate the spin dynamics during frequency-swept pulses that are relevant to the spatial encoding process. All the simulations were carried out with the SPINACH software library [29], implemented in MATLAB; version 2.3 was used. SPINACH uses the Fokker-Planck formalism to account simultaneously for spin and spatial variables, and provides an efficient tool for the simulation of ultrafast NMR experiments [30, 31], including relaxation and diffusion effects. The details of the simulation framework are not described here and can be found in Refs [30, 31]. Other approaches to the description of spin dynamics during frequency-swept pulses have been described by Foroozandeh [32].

Systems of homonuclear spins $I = 1/2$ were considered here. The time evolution of the density operator under the effect

of a frequency-swept pulse and a magnetic field gradient was calculated with SPINACH, including the effect of chemical-shifts, J couplings, and, optionally, translational molecular diffusion and relaxation. Linearly swept chirp pulses, were used in all the simulations, with a WURST envelope [26]. Further details of the simulation are given in the figure captions.

A system of N homonuclear spins $I = 1/2$, for a volume element at position z may be described by a density operator:

$$\sigma(z,t) = \sum_{r=1}^{2^{2N}} b_r(z,t) B_r, \tag{8}$$

where B_r is a basis set of orthogonal operators that all have the same norm, and $b_r(z,t)$ the coefficient of the expansion of σ in that basis.

The squared norm of the density operator is:

$$\|\sigma(z,t)\|^2 = \|B_1\|^2 \sum_{r=1}^{2^{2N}} |b_r(z,t)|^2. \tag{9}$$

To visualise the spin dynamics, selected trajectories were formed here by calculating the quantities:

$$A_S(z,t) = \sum_{r \in S} |b_r(z,t)|^2, \tag{10}$$

where S is a subset of operators.

The result of the spatial encoding process was also visualised by considering the magnitude and phase of the expectation value of specific operators:

$$\frac{\langle B_r \rangle(r,t)}{\|B_r\|^2} = \frac{\langle B_r | \sigma(r,t) \rangle}{\|B_r\|^2} = b_r(z,t). \tag{11}$$

5. Exact and approximate spin dynamics of spatial encoding

5.1. Instantaneous flip approximation

The implementation, setup and analysis of ultrafast NMR experiments requires a description of the spins' evolution during frequency-swept pulses. Most analyses of ultrafast NMR experiments rely on the assumption of instantaneous rotation of the spins when the frequency of the swept pulse matches that of the nuclear spins [33, 34]. The origin of this approximation can be illustrated with the case of chirp pulses.

Consider an ensemble of uncoupled nuclear spins $I = 1/2$ that have a chemical-shift offset $\Omega_i = -\gamma B_0(1-\sigma_i) - \omega_R$, where ω_R is the rotation rate of the rotating frame of reference, B_0 is the static magnetic field, and σ_i is the chemical shielding, placed in a magnetic-field gradient $\mathbf{G} = G\mathbf{e}_z$ ($\mathbf{e}_z$ is a unit vector along z). The total frequency offset of the spins is, at position z:

$$\omega_i = \Omega_i - \gamma G z. \tag{12}$$

A basis set for single-spin system is given in Table 1. Figure 5 shows the time evolution of the magnetisation at different positions during the application of a 180° chirp pulse of duration T_e and sweep rate R, in the presence of a magnetic field gradient of intensity G, for two cases. In the case of an initially longitudinal magnetisation (Fig. 5a), the initial density operator is I_{1z} and the plotted quantity is the coefficient of I_{1z} in the density operator. In the case of an initially transverse magnetisation (Fig. 5b), the initial density operator is $1/\sqrt{2} I_{1+}$ and the plotted quantities are

Table 1: Basis set of product operators for a single spin system

1:	$\frac{1}{2}E$	2:	$\frac{1}{\sqrt{2}}I_{1+}$	3:	I_{1z}	4:	$\frac{1}{\sqrt{2}}I_{1-}$

$$A_+ = |b_2|^2, \tag{13}$$

and

$$A_- = |b_4|^2, \tag{14}$$

corresponding the amount of +1 and -1 coherences, respectively. It can be seen in Fig. 5 that the flip occurs sequentially across the sample. The rotation is, however, not instantaneous and it takes here about one third of the pulse duration for 90% of the magnetisation to rotate. There are also oscillations before and after the flip. In spite of these observations, an excellent agreement is obtained between the result of the exact spin dynamics and approximate models based on the assumption of an instantaneous flip, as will be shown in section 6. The trajectories shown in Fig. 5 depend on the adiabaticity factor, and on the product of the pulse duration to its bandwidth (the so-called time-bandwidth product $TBW = T_e \times BW$), and it is found empirically that the instantaneous-flip approximation breaks down for $TBW < 50$ [35].

The spins are expected to flip at a time t_{flip} such that the frequency of RF field is equal to that of the nuclear spins:

$$\omega_{\text{rf}}(t_{\text{flip}}) = \omega_i. \tag{15}$$

In the case of a chirp pulse, this condition gives:

$$t_{\text{flip}} = \frac{\omega_i - \omega_{\text{rf}}^0}{R}. \tag{16}$$

Figure 5c shows a comparison between this analytical expression and the flip time calculated from numerical simulations in the case of an initially transverse magnetisation, defined as the time when $A_+(t_{\text{flip}}^{\text{sim}}) = A_-(t_{\text{flip}}^{\text{sim}})$. The analytical expression of Eq. 16 is in agreement with the result of simulation.

With this model, spatial encoding of longitudinal relaxation is analysed by assuming that the recovery delay is $T_e - t_{\text{flip}}(z)$. For spatial encoding of chemical shifts and diffusion coeffcients, a calculation of the phase variation, after a 180° frequency-swept pulse is applied to an initially transverse magnetisation, is necessary to analyse the results.

5.2. Phase

The phase at the end of a frequency-swept 180° pulse, assuming an instantaneous flip, can be calculated as follows. The phase just before the flip is:

$$\phi\left(t_{\text{flip}}^-\right) = \phi_0 + \omega_i t_{\text{flip}}. \tag{17}$$

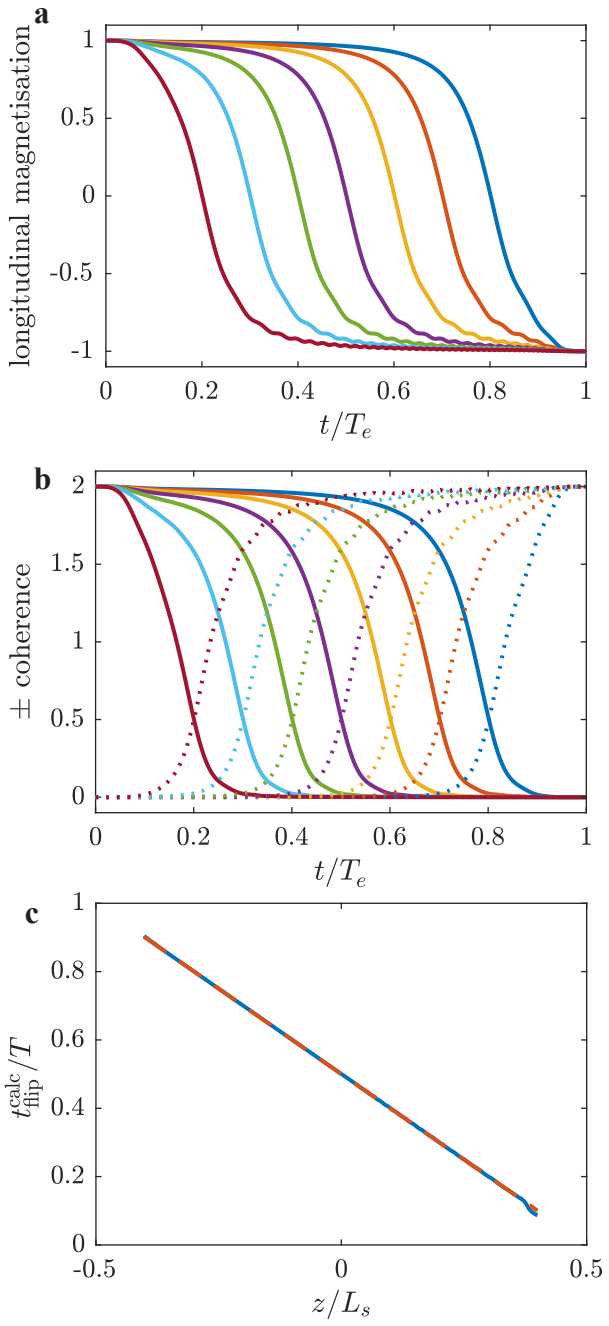

Figure 5: (a-b) Trajectories of the spins for several slices, during a frequency-swept pulse applied in the presence of a magnetic field gradient, and (c) comparison between the numerical (blue) and approximate analytical (orange, Eq. 16) flip time. In (a), the coefficient of the longitudinal magnetisation is shown, for an initial state that consists of longitudinal magnetisation. In (b), the amount of +1 (solid) and −1 (dotted) coherence is shown, for an initial state that consists of +1 coherence. The simulated pulse has an adiabaticity factor $Q = 6.28$ and a time-bandwidth product $TBW = 150$, and is applied in the presence of a magnetic field gradient $G = RT_e/(\gamma L_s)$. Trajectories are shown for 7 different slices, located at $i \times L_s/10$, for i ranging from 2 (blue) to 8 (dark red).

and the phase at the end of the pulse is:

$$\phi\left(T_e\right) = \phi\left(t_{\mathrm{flip}}^{+}\right) + \omega_i\left(T_e - t_{\mathrm{flip}}\right). \tag{18}$$

The difference in phase before and after the flip results from a 180° rotation of the magnetisation around the RF field:

$$\phi\left(t_{\mathrm{flip}}^{+}\right) - \phi\left(t_{\mathrm{flip}}^{-}\right) = 2\left(\phi_{\mathrm{rf}}(t_{\mathrm{flip}}) - 2\phi\left(t_{\mathrm{flip}}^{-}\right)\right), \tag{19}$$

where ϕ_{rf} is the phase of the RF field. Combining Eqs 17, 18 and 19 gives:

$$\phi\left(T_e\right) = -\phi_0 + 2\phi_{\mathrm{rf}}\left(t_{\mathrm{flip}}\right) + \omega_i\left(T_e - 2t_{\mathrm{flip}}\right). \tag{20}$$

In this equation, no assumption is made on the specific form of the RF frequency sweep or of the spins's frequency offset.

5.3. Derivative of the phase

Spatial encoding experiments rely on the position-dependence of the derivative of the phase, with respect to chemical shift in the case of chemical shift encoding (UF 2D NMR), with respect to position in the case of diffusion encoding (UF DOSY and LNMR). Before the flip, the derivative with respect to α, which may be the chemical-shift offset or position, is:

$$\frac{\partial\phi}{\partial\alpha}(t) = \frac{\partial\phi_0}{\partial\alpha} + \frac{\partial\omega_i}{\partial\alpha}t \quad \text{for} \quad t < t_{\mathrm{flip}}. \tag{21}$$

Valette *et al.* have shown that the calculation of this derivative after the flip need not take into account the phase of the RF pulse at the time of the flip [36]. Eq. 20 is valid for times $t > t_{\mathrm{flip}}$, taking the derivative with respect to α:

$$\begin{aligned}\frac{\partial\phi}{\partial\alpha}(t) \quad = \quad & -\frac{\partial\phi_0}{\partial\alpha} + 2\frac{\partial t_{\mathrm{flip}}}{\partial\alpha}\frac{\partial\phi_{\mathrm{rf}}}{\partial t}\left(t_{\mathrm{flip}}\right) \\ & + \frac{\partial\omega_i}{\partial\alpha}\left(t - 2t_{\mathrm{flip}}\right) - 2\omega_i\frac{\partial t_{\mathrm{flip}}}{\partial\alpha}\end{aligned} \tag{22}$$

The flip time is defined by the condition $\omega_i = \omega_{\mathrm{rf}} = \partial\phi_{t_{\mathrm{flip}}}/\partial t$, so that the second and fourth term on the right-hand side of Eq. 22 cancel out:

$$\frac{\partial\phi}{\partial\alpha}(t) = -\frac{\partial\phi_0}{\partial\alpha} + \frac{\partial\omega_i}{\partial\alpha}\left(t - 2t_{\mathrm{flip}}\right) \quad \text{for} \quad t > t_{\mathrm{flip}}. \tag{23}$$

Again in this equation no assumption is made on the form of the RF frequency sweep or of the spins' frequency offset. It can provide a useful route to the analysis of diffusion and chemical-shift encoding methods.

5.4. Case of the chirp pulse

The phase at the end of a 180° chirp pulse can be obtained by combining equations 20, 5, and 16:

$$\phi\left(T_e\right) = -\phi_0 + T_e\omega_i - \frac{\left(\omega_i - \omega_{\mathrm{rf}}^0\right)^2}{R}. \tag{24}$$

For a pulse that sweeps symmetrically around 0 in the rotating-frame of reference ($\omega_{\mathrm{rf}}^i = -RT_e/2$):

$$\phi\left(T_e\right) = -\phi_0 - \frac{1}{4}RT_e^2 - \frac{\omega_i^2}{R}. \tag{25}$$

A linearly frequency-swept pulse yields a phase variation that is quadratic with respect to the frequency offset of the spins during the sweep.

Replacing ω_i in Eq. 24 by the right hand-side of Eq. 12 gives the phase at the end of the chirp pulse for uncoupled spins in a magnetic field gradient:

$$\begin{aligned}\phi(z,T_e) &= -\phi_0(z) - \left(\frac{(\gamma G)^2}{R}\right) z^2 \\ &\quad - \left(\frac{2\gamma G\left(\omega_{\mathrm{rf}}^0 - \Omega_i\right)}{R} + \gamma G T_e\right) z \\ &\quad + \left(T_e\Omega_i - \frac{\left(\omega_{\mathrm{rf}}^i - \Omega_i\right)^2}{R}\right). \end{aligned} \tag{26}$$

Considering a symmetric sweep with $\omega_{\mathrm{rf}}^i = -RT_e/2$:

$$\begin{aligned}\phi(z,T_e) &= -\phi_0(z) - \frac{(\gamma G)^2}{R} z^2 \\ &\quad + \frac{2\gamma G\Omega_i}{R} z \\ &\quad - \frac{\Omega_i^2}{R} - \frac{1}{4} R T_e^2. \end{aligned} \tag{27}$$

The non-linear spatial phase variation that results from the joint application of a frequency-swept pulse and a magnetic-field gradient pulse is not compatible with classic acquisition schemes. It was shown numerically and experimentally by Kunz that this quadratic phase variation can be refocused by the application of a second, identical frequency-swept pulse [37, 38]. Most implementations of spatial encoding of chemical shifts or diffusion (UF 2D NMR, UF DOSY, UF LNMR) thus rely on a pair of frequency-swept pulses, as illustrated in Fig. 2b and c.

In the case of 180° chirp pulses, the phase variation after the pulse is quadratic with respect to ω_i, as shown in section 5.2. When a pair of 180° pulses is applied, with identical duration and sweep rate, using field-gradient strength G for the first pulse and $G' = \pm G$ for the second pulse, the spatially quadratic phase cancels out, yielding, for a symmetric sweep ($\omega_{\mathrm{rf}}^i = -RT_e/2$):

$$\phi^{\pi,\pi}(z) = \phi_0(z) - 2\frac{\gamma G}{R}(1 - \mathrm{sgn}(G'))\Omega_i z. \tag{28}$$

Equations 27 and 28 are useful for the analysis of UF 2D NMR, UF DOSY, and UF LNMR experiments.

6. Spatial encoding

6.1. Encoding of relaxation rates

Ultrafast inversion-recovery experiments map the recovery delay of IR experiments onto a spatial axis, using a frequency-swept pulse. A pulse-sequence element for relaxation spatial encoding is shown in Fig. 2a. In the instantaneous flip approximation, the recovery delay is $T_e - t_{\mathrm{flip}}(z)$ at position z and the magnetisation at the end of the pulse is:

$$\frac{M_z(z)}{M_z^0} = 1 - 2\exp\left(-R_1\left(T_e - t_{\mathrm{flip}}(z)\right)\right), \tag{29}$$

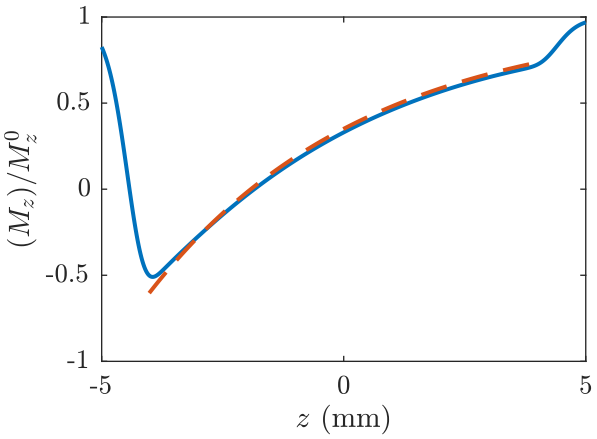

Figure 6: Spatial encoding of relaxation. The blue solid line shows the simulated longitudinal magnetisation after the application, to the thermal equilibrium magnetisation, of a frequency-swept chirp pulse of duration 150 ms and bandwidth 1 kHz, together with a magnetic field gradient of 0.23 G/cm. The pulse sweep over a spatial region of 10 mm. The simulation accounts for nuclear spin relaxation with relaxation rate of $R = 15\ \mathrm{s}^{-1}$, and uses a DiBari-Levitt description of thermalisation [39]. The red dashed line shows the analytical expression $1 - 2\exp(-R_1(T_e - t_{\mathrm{flip}}(z)))$.

where R_1 is the longitudinal relaxation rate.

Figure 6 shows a comparison between this analytical expression and the result of numerical simulation for a pulse that sweeps over a region of 10 mm in 150 ms, with a bandwidth of 1 kHz. The agreement is very good and in practice relaxation rates are obtained by modelling the data of UF IR experiments with Eq. 29. The pulse duration should be several times longer than the longest relaxation rate of interest.

The simulated data also reflects the time-envelope of the frequency-swept pulse used for spatial encoding. This is not accounted for in the analytical model, and this is why the comparison is shown for the region where the time-enveloppe of the pulse is approximately constant.

6.2. Encoding of chemical shifts

Ultrafast 2D NMR experiments map the evolution delay of 2D experiments onto a spatial dimension and thus require a phase variation of the form $C\Omega_i z$, where C is the spatial encoding constant. When a 180° chirp pulse is applied in combination with a magnetic field gradient pulse to an initially transverse magnetisation, the chemical-shift spatial-encoding phase is given, in the instantaneous-flip approximation, by the chemical-shift dependent terms on the right-hand side of Eq. 27. In UF 2D NMR pulse sequences a pair of pulses is used, with $G' = -G$, to remove the spatially quadratic phase while doubling the chemical-shift spatial-encoding phase. Figure 2b shows a pulse sequence element for chemical-shift spatial encoding. Defining the length of the spatial region swept by the pulse as $L_s = RT_e/(\gamma G)$, the phase at the end of the spatial encoding block is:

$$\phi_{\mathrm{UF,CS}} = -4\Omega_i T_e \frac{z}{L_s}. \tag{30}$$

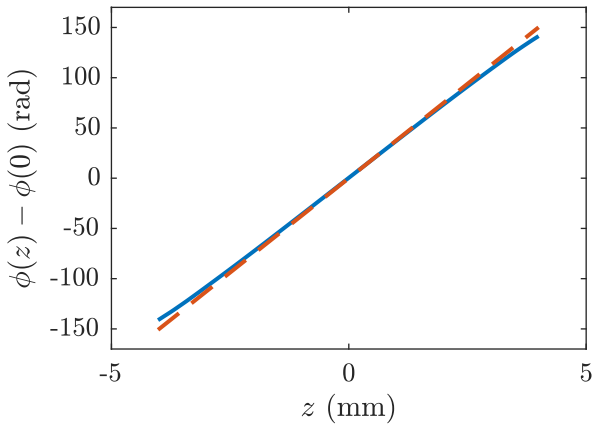

Figure 7: Spatial encoding of the chemical shift, for uncoupled spins. The blue solid line shows the simulated phase after the application, to an initial state I_{1+}, of a pair of frequency-swept chirp pulses of duration 15 ms each and bandwidth 10 kHz, together with bipolar magnetic field gradient pulse of ±2.3 G/cm. The pulses sweep over a spatial region of 10 mm. The simulation accounts for a chemical-shift frequency offset of $\Omega/(2\pi) = 1$ kHz. The red dashed line shows the analytical expression $4(\gamma G/R)\Omega_1 z$.

Figure 7 shows a comparison between Eq. 30 and the result of numerical simulation for the application of a pair of chirp pulse of 15 ms each that sweeps over a region of 10 mm, with a bandwidth of 10 kHz, for uncoupled spins with a chemical-shift frequency offset of 1 kHz. Such pulse duration would typically be used to achieve a compromise between resolution and spectral width in the spatially encoded dimension [17]. There is very good agreement between the two, and the spatial encoding block shown in Fig. 2b forms the basis of most UF 2D NMR experiments [33, 17, 24].

The chemical-shift spatial-encoding phase imparted by a chirp pulse may also be derived with a simpler analysis, by assuming that spins precess under the effect of the chemical shift during a time $\left(T_e - 2t_{\text{flip}}\right)$. This may be understood by combining Eq. 23, with $\alpha = \Omega_i$, Eq. 12 and Eq. 16:

$$\begin{aligned}\frac{\partial(\phi-\phi_0)}{\partial\Omega_i}(T_e) &= T_e - 2t_{\text{flip}} \\ &= -2\frac{\Omega_i}{R} + 2\frac{\gamma G z}{R}\end{aligned} \tag{31}$$

Introducing the length of the spatial region swept by the pulse:

$$\frac{\partial(\phi-\phi_0)}{\partial\Omega_i}(T_e) = 2\frac{T_e}{L_s}\left(z - \frac{\Omega_i}{\gamma G}\right) \tag{32}$$

Equation 32 corresponds to an effective evolution time that ranges linearly from $-T_e$ to T_e over the spatial region of length L_s. This region is shifted by $\Omega_i/(\gamma G)$ for spins with chemical-shift offsets Ω_i.

Note that with the spatial encoding block shown in Fig. 2b, the chemical shift displacements of the regions swept by the pulses have opposite signs for the two sweeps $\Omega_i/(\pm\gamma G)$. Eventually, for a given chemical shift offset, only the fraction of the sample that experiences both sweeps contributes to the signal. This results in a small chemical-shift dependence of the lineshape and intensity in UF 2D NMR experiments, and is the reason why the bandwidth of the chirp pulse should be large enough compared to the spectral region of interest. A factor of 5 is empirically found to be sufficient [40].

Similar results can be achieved with the combination of magnetic-field gradient pulses and chirp excitation pulses [6, 7]. In this case the frequency-swept pulse is operated outside the adiabatic regime, with a power chosen to achieve a flip angle of 90°. However, 90° chirp pulses are more difficult to calibrate [41] and the resulting spatial encoding schemes were found to be less efficient [42].

6.3. Encoding of diffusion coefficients

Ultrafast diffusion NMR experiments map the gradient area of diffusion NMR experiments onto a spatial dimension. This is achieved with a pair of chirp pulses separated by a diffusion delay Δ, and applied together with magnetic field gradient pulses. The condition $G' = G$ is used, so that the phase variation imparted by the first pulse is fully refocussed by the second one, and the diffusion information is encoded through a position-dependent attenuation of the transverse magnetisation.

Figure 2c shows a pulse sequence element for diffusion spatial encoding. The spatially resolved signal measured in ultrafast DOSY or LNMR experiments can, in analogy the Stejskal-Tanner equation [43], be modelled as:

$$\frac{S(z)}{S_0} = \exp\left(-D\Delta'(K(z, 2T_e))^2\right), \tag{33}$$

where Δ' is the effective diffusion time, that accounts for the finite width of the diffusion-encoding gradients [44, 36, 45], and K is a position dependent effective gradient area multiplied by the gyromagnetic ratio. Several approaches have been described to derive Eq. 33, based on the Bloch-Torrey equation or on a propagator description of the pulse sequence [46].

6.3.1. Bloch-Torrey model

Consider an ensemble of uncoupled nuclear spins in a volume element that experiences a time-dependent magnetic-field gradient of the form $\mathbf{G}(t) = G(t)\mathbf{e}_z$. The effect of translational molecular diffusion on the transverse magnetisation is given by the following solution of the Bloch-Torrey equation [46]:

$$\begin{aligned}|M_{xy}(t)| &= |M_{xy}(0)|\exp\left(-\frac{t}{T_2}\right) \\ &\quad\times\exp\left(-D\int_0^t (k(t'))^2 dt'\right),\end{aligned} \tag{34}$$

where

$$k(t) = \gamma\int_0^t G(t')dt'. \tag{35}$$

This expression can be generalised to the case of arbitrary spatial variations of the phase as shown, e.g., in Ref. [47, 36, 44], by replacing the gradient area by the spatial derivative of the phase:

$$\begin{aligned}|M_{xy}(t)| &= |M_{xy}(0)|\exp\left(-\frac{t}{T_2}\right) \\ &\quad\times\exp\left(-D\int_0^t (K(z,t'))^2 dt'\right)\end{aligned} \tag{36}$$

where

$$K(z,t) = \frac{\partial\phi(z,t)}{\partial z}. \tag{37}$$

Equation 36 is valid in the limit where the diffusion length is small enough for the phase variation experienced by the spins during the diffusion time to be linear. For chirp pulses this translates into the condition [36]:

$$\lambda^2 = 2D\Delta \ll \frac{\pi R}{\gamma^2 G^2}, \tag{38}$$

where λ^2 is the mean squared displacement of the spins during the diffusion time. Two methods have been described to calculate K, either analytically or numerically.

Instantaneous-flip approximation. Using the instantaneous-flip approximation, the value of $K(z,t)$ can be calculated for a frequency-swept pulse that follows an excitation pulse, using Eqs 21 and 23:

$$K(z,t) = -\gamma G t \quad \text{for} \quad t < t_{\text{flip}}. \tag{39}$$

$$K(z,t) = -\gamma G\left(t - 2t_{\text{flip}}(z)\right) \quad \text{for} \quad t > t_{\text{flip}}. \tag{40}$$

In the case of a chirp pulse, this gives:

$$K(z,t) = -\gamma G\left(t - 2\frac{\Omega_i - \omega^0_{\text{rf}} - \gamma G z}{R}\right) \quad \text{for} \quad t > t_{\text{flip}}. \tag{41}$$

In UF DOSY and LNMR pulse sequences, an additional gradient pulse of duration T_e is typically applied after the chirp+gradient block. This gives, for a symmetric sweep ($\omega^0_{\text{rf}} = -RT_e/2$):

$$K(z,2T_e) = -2\gamma G T_e\left(\frac{1}{2} + \frac{z - \Omega_i/(\gamma G)}{L_s}\right) \tag{42}$$

This expression corresponds to a mapping of the effective gradient-encoding duration onto a spatial dimension, from 0 to $2T_e$ over a spatial region of length L_s. Without the extra gradient, the effective duration of the gradient ranges from $-T_e$ to T_e and redundant information is encoded.

The spatial-encoding region is shifted by $\Omega_i/(\gamma G)$ for spins with chemical-shift offset Ω_i. A full calculation for a pair of chirp+gradient block separated by a diffusion delay Δ, as shown in Fig. 2, yields $\Delta' = \Delta - T_e$: diffusion during the finite pulses results in a decrease of the effective diffusion time by T_e.

Figure 8 shows a comparison between numerical simulation of the pulse sequence element shown in Fig. 2c, and of the analytical expression given in Eq. 33. There is good agreement between the two, which is further improved by correcting for the spatial profile of the chirp [31]. For a given length of the encoded region, the maximum attenuation is defined by the time-bandwidth product of the chirp pulse.

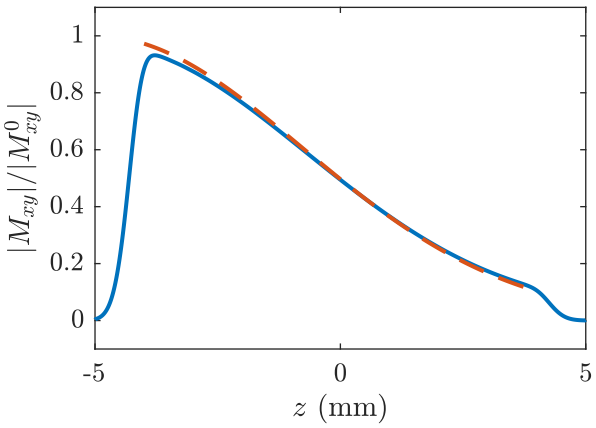

Figure 8: Spatial encoding of diffusion.The blue solid line shows the simulated longitudinal magnetisation after the application, to an initial state I_{1z}, of the pulse sequence element shown in Fig. 2, with a duration of 1.5 ms and a bandwidth of 100 kHz for the chirp pulses, and an amplitude of 23 G/cm for the gradient pulses. The pulse sweep over a spatial region of 10 mm. The simulation accounts for translational diffusion with a diffusion coefficient of $D = 10\ \text{m}^2 \cdot \text{s}^{-1}$. The red dashed line shows the analytical expression $\exp(-D(\Delta - T_e)(\gamma G(2(T_e - t_{\text{flip}}(z))))^2)$.

Numerical integration. The phase variation after the combination of a chirp pulse and a magnetic field gradient can also be calculated exactly, by numerical integration [4]. In a reference frame that rotates at the frequency of the swept pulse, the precession frequency of the spins is, during the pulse:

$$\omega_{\text{eff}}(t,z) = \sqrt{(\Omega_i - \gamma G z - \omega_{\text{rf}}(t))^2 + (\gamma B_1(t))^2} \tag{43}$$

where B_1 is the strength of the RF field. The phase variation at the end of the pulse is:

$$\phi(z,T_e) = \int_0^{T_e} \omega_{\text{eff}}(z,t)dt. \tag{44}$$

which gives, for a chirp pulse of duration T_e followed by an additional gradient of duration T_e:

$$K(z,2T_e) = \int_0^{T_e} \frac{d\omega_{\text{eff}}(z,t)}{dz}dt + \gamma G T_e. \tag{45}$$

With this approach, diffusion during the frequency-swept pulse is not accounted for; this is valid for $\Delta \gg T_e$. An empirical correction to the diffusion time, $\Delta' = \Delta - T_e$, can be used based on the result obtained with the instantaneous-flip approximation. This model was found to give the best agreement with numerical simulation [45].

6.3.2. *Propagator model*

The effect of translational molecular diffusion may also be calculated using a propagator model [46], that accounts for the phase difference $\Phi(Z)$ for particles that experience a displacement $Z = z - z_0$ in an echo experiment, where z_0 is the position during the dephasing gradient and z is the position during the rephasing gradient. The echo amplitude is given by:

$$E(z) = \int P(Z,\Delta)\exp\left(i\Phi(Z)\right)dZ, \tag{46}$$

where

$$P(Z,\Delta) = \frac{1}{\sqrt{4\pi D\Delta}} \exp\left(-\frac{Z^2}{4D\Delta}\right) \quad (47)$$

is the average propagator for free diffusion, and Δ is the diffusion time. Ahola *et al.* have used this model to analyse single-scan PGSE and PGSTE pulse sequence [48]. For a pair of chirp+gradient blocks separated by a diffusion delay, the phase difference Φ is calculated from Eqs 27, neglecting chemical-shift offsets and assuming $\phi_0 = 0$:

$$\Phi(Z) = -\frac{\gamma^2 G^2}{R}\left(z^2 - z_0^2\right) - \gamma G T_e (z - z_0). \quad (48)$$

$$(49)$$

Since

$$\begin{aligned} z^2 - z_0^2 &= (z + z_0)(z - z_0) \\ &= (2z + z_0 - z)(z - z_0) \\ &= (2z - Z)Z, \end{aligned} \quad (50)$$

one has:

$$\Phi(Z) = -\gamma G T_e Z - 2\frac{\gamma^2 G^2}{R} zZ + \frac{\gamma^2 G^2}{R} Z^2. \quad (51)$$

Assuming, as in section 6.3.1, that the squared dynamic displacement Z^2 is much smaller than $\pi R/(\gamma^2 G^2)$, the third term on the right hand-side of Eq. 51 is negligible and one has::

$$\begin{aligned} \Phi(Z) &= -2\gamma G T_e Z\left(\frac{1}{2} + \frac{z}{L_s}\right) \\ &= ZK(z, 2T_e) \end{aligned} \quad (52)$$

Combining Eqs 46, 47 and 52:

$$E(z) = \exp\left(-D\Delta\left(K(z, 2T_e)\right)^2\right). \quad (53)$$

which is the same expression as Eq. 33. In this model, however, it is assumed that diffusion during the chirp + gradient blocks is negligible. The finite width of these blocks can be accounted for by using an empirically corrected diffusion time Δ'.

7. Systems of J-coupled spins

While most descriptions of spatial encoding in UF 2D NMR rely on a vector model for uncoupled spins, a majority of experiments concern spin systems for which scalar couplings are present and active during the spatial encoding process [33, 17]. Also, several experiments have been reported that rely on the spatial encoding of multiple-quantum chemical shifts [49, 50, 51, 52]. A simple analytical description can be given for systems of weakly coupled spins, based on the same assumptions as for uncoupled spins.

Table 2: Basis set of product operators for a two-spin system

1:	$\frac{1}{2}E$	5:	$\frac{1}{\sqrt{2}}I_{1+}$	9:	I_{1z}	13:	$\frac{1}{\sqrt{2}}I_{1-}$
2:	$\frac{1}{\sqrt{2}}I_{2+}$	6:	$I_{1+}I_{2+}$	10:	$\sqrt{2}I_{1z}I_{2+}$	14:	$I_{1-}I_{2+}$
3:	I_{2z}	7:	$\sqrt{2}I_{1+}I_{2z}$	11:	$2I_{1z}I_{2z}$	15:	$\sqrt{2}I_{1-}I_{2z}$
4:	$\frac{1}{\sqrt{2}}I_{2-}$	8:	$I_{1+}I_{2-}$	12:	$\sqrt{2}I_{1z}I_{2-}$	16:	$I_{1-}I_{2-}$

7.1. Instantaneous flips in multi-spin systems

For systems of homonuclear weakly coupled spins, the effect of the joint application of a 180° chirp pulse and a magnetic field gradient can be described by considering independent flip times for each nuclear spin (or group of equivalent nuclear spins). Consider for example an AX system of 2 homonuclear weakly coupled spins 1 and 2, of chemical shift offsets Ω_1 and Ω_2, that experiences a chirp pulse of duration T_e, sweep rate R, and initial frequency offset $\omega_{\rm rf}^0 = -RT_e/2$, with a magnetic field gradient G. The effect of the J coupling on the flip time is negligible and the flip times for the two spins are:

$$t_{\rm flip}^{(1)} = \frac{\Omega_1 - \gamma G z - \omega_{\rm rf}^0}{R}, \quad (54)$$

and

$$t_{\rm flip}^{(2)} = \frac{\Omega_2 - \gamma G z - \omega_{\rm rf}^0}{R}. \quad (55)$$

The two coupled nuclear spins in a given position do not experience the rotation at the same time, and the flip times differ by $\Delta t_{\rm flip} = (\Omega_1 - \Omega_2)/R$.

This result can be illustrated with numerical simulations of the spin dynamics during the combined application of frequency-swept pulse and a magnetic field gradient. A basis set for a two-spin system is given in Table 2. Figure 9 shows selected trajectories for several initial operators, for a chemical-shift difference of 500 Hz and a J coupling of 17 Hz.

In order to illustrate the dynamics relevant for, e.g., COSY experiments, Fig. 9 shows, for an initial single-quantum operator $\sigma(0) = I_{1\alpha}I_{2+}$ and for several values of the position z, the quantities:

$$A_{2+}(t) = \sum_{r\in\{2,6,10,14\}} |b_r|^2, \quad (56)$$

and

$$A_{2-}(t) = \sum_{r\in\{4,8,12,16\}} |b_r|^2, \quad (57)$$

corresponding to the amount of +1 and −1 coherences for spin 2, irrespective of the state of spin 1, and

$$A_{1z}(t) = \sum_{r\in\{9,10,11,12\}} |b_r|^2 \quad (58)$$

corresponding to the amount of longitudinal order for spin 1, irrespective of the state of spin 2. Comparing the curves for spins 1 and 2, one can see that they flip at different times. Defining the flip time as $A_{2+}(t_{\rm flip}^{(2)}) = A_{2-}(t_{\rm flip}^{(2)})$ for spin 2 and $A_{1z}(t_{\rm flip}^{(1)}) = 0$ for spin 1, the results from numerical simulation can be compared

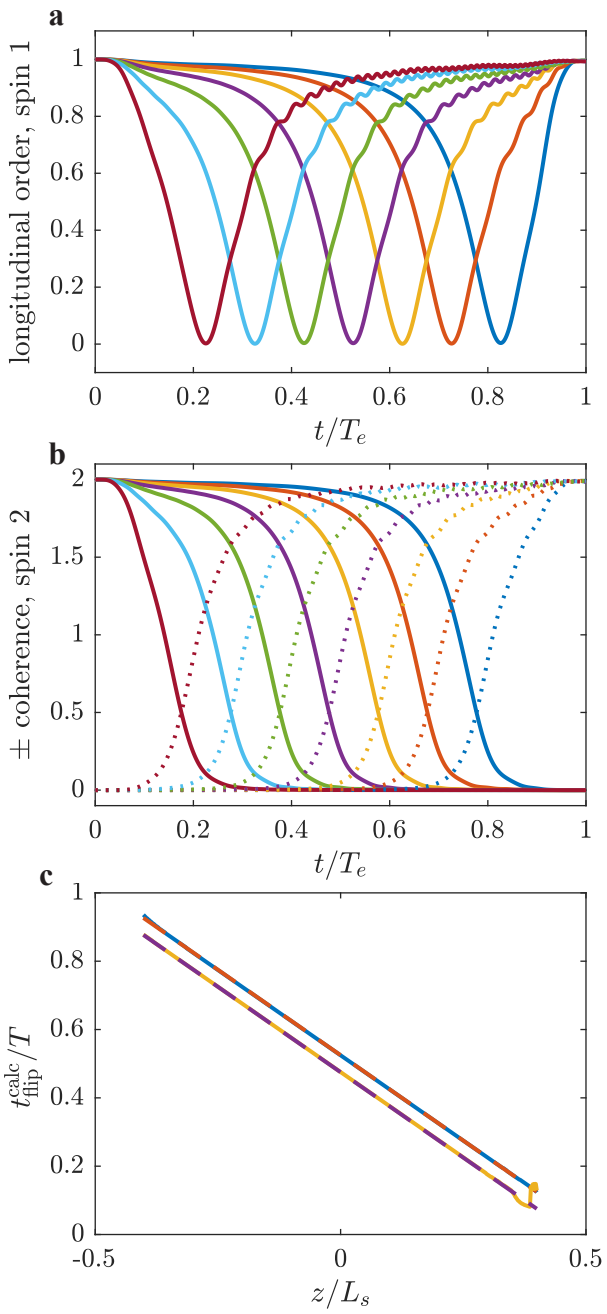

Figure 9: (a, b) Trajectories of the spins for several slices, so an initial single-quantum operator $\sqrt{2}I_{1\alpha}I_{2+}$, during a frequency-swept pulse applied together with a magnetic field gradient, for a two-spin system, and (c) comparison between the numerical (solid) and approximate analytical (dashed) flip time for spins 1 (blue and yellow) and 2 (red and purple). In (a), the amount of longitudinal order for spin 1 is shown. In (b), the amount of +1 (solid) and −1 (dotted) coherence is shown for spin 2. The simulated pulse has an adiabaticity factor $Q = 6.28$ and a time-bandwidth product $TBW = 150$, and is applied together with a magnetic field gradient $G = RT_e/(\gamma L_s)$. The two spins have a chemical-shift frequency offset of $\pm RT_e/(40 \times 2\pi)$, and a mutual J coupling of $1/(4T_e)$. Trajectories are shown for 7 different slices, located at $i \times L_s/10$, for i ranging from 2 (blue) to 8 (dark red).

to the approximate analytical expressions. Figure 9 shows a comparison between the flip time as a function of z calculated by numerical simulation, and Eqs 54 and 55. The two are in excellent agreement. The simulated values for spin 1 near $z/L_s = 0.4$ correspond to a region of unencoded magnetisation, because of the chemical-shift-induced spatial offset.

The dynamics relevant for multiple-quantum coherences are shown in Fig. 10, where an initial operator $\sigma(0) = I_{1+}I_{2+}$ is used, and the plotted quantities are A_{2+}, A_{2-},

$$A_{1+}(t) = \sum_{r\in\{5,6,7,8\}} |b_r|^2, \tag{59}$$

and

$$A_{1-}(t) = \sum_{r\in\{13,14,15,16\}} |b_r|^2. \tag{60}$$

Again, it can be seen that spins 1 and 2 flip independently at well-defined times, which are given by Eqs 54 and 55. These results are useful to describe spatial encoding in multi-spin systems.

7.2. *Spatial encoding of multiple-quantum chemical-shifts*

For multiple-quantum coherences, the total phase variation after a chirp + gradient block is simply equal to the sum of the single-spin phase variations, weighted by the coherence order. For an operator of the form

$$B = \prod_{i=1}^{p} I_{i\epsilon_i}, \tag{61}$$

where p is the number of spins involved, and ϵ_i is either + or −, the phase after the application of a 180° chirp pulse and a magnetic field gradient is:

$$\phi_{\mathrm{mq}}(z, T_e) = \sum_i \epsilon_i \phi_i(z, T_e), \tag{62}$$

with

$$\phi_i(z, T_e) = -\frac{(\gamma G)^2}{R} z^2 + \frac{2\gamma G \Omega_i}{R} z - \frac{\Omega_i^2}{R} - \frac{1}{4} R T_e^2. \tag{63}$$

In UF 2D NMR experiments, the phase variation after the application of two 180° chirp pulses applied with bipolar gradients is:

$$\phi^{\pi,\pi}(z) = -4\frac{\gamma G}{R}\left(\sum_i \epsilon_i \Omega_i\right) z. \tag{64}$$

This is illustrated in Fig. 11 with the example of a double-quantum coherence. Equation 64 is a simple extension of Eq. 30. As a result, the ultrafast version of multidimensional experiments that involve multiple-quantum coherences in the indirect dimension can be implemented simply by applying a spatial encoding block instead of the incremented evolution delay.

The expression given in Eq. 62 also explains the mechanisms through which the contribution of zero-quantum coherences is suppressed by the filter described by Thrippleton and Keeler [19], as well as the suppression of coherence transfer pathways in the PSYCHE method for homonuclear decoupling [20].

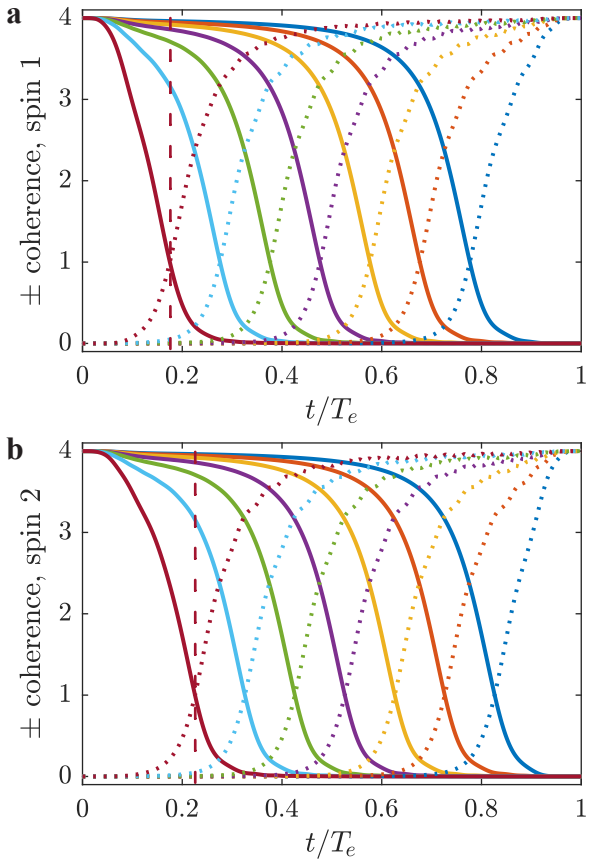

Figure 10: Trajectories of the spins for several slices, during a frequency-swept pulse applied together with a magnetic field gradient, for a two-spin system. The initial state is $I_{1+}I_{2+}$. In (a), the amount of +1 (solid) and −1 (dotted) coherence is shown for spin 1. In (b), the amount of +1 (solid) and −1 (dotted) coherence is shown for spin 2. Vertical dashes lines indicate the flip times of spins 1 and 2 in one of the slices. The simulated pulse has an adiabaticity factor $Q = 6.28$ and a time-bandwidth product $TBW = 150$, and is applied together with a magnetic field gradient $G = RT_e/(\gamma L_s)$. The two spins have a chemical-shift frequency offset of $\pm RT_e/(40 \times 2\pi)$, and a mutual J coupling of $1/(4T_e)$. Trajectories are shown for 7 different slices, located at $i \times L_s/10$, for i ranging from 2 (blue) to 8 (dark red).

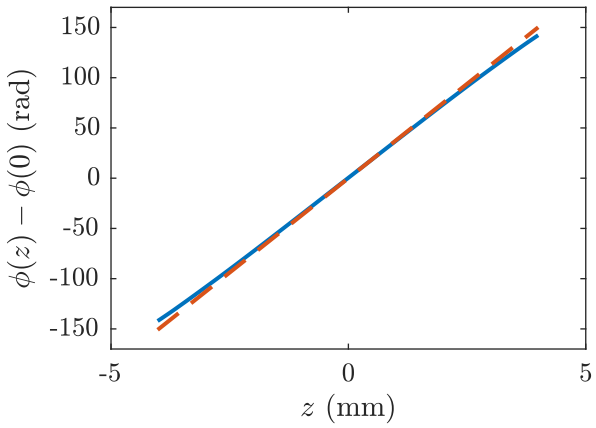

Figure 11: Spatial encoding of the chemical shift, for a pair of J-coupled spins. The blue solid line shows the simulated phase after the application, to an initial state $I_{1+}I_{2+}$, of a pair of frequency-swept chirp pulses of duration 15 ms and bandwidth 10 kHz, together with bipolar magnetic field gradient pulse of ±2.3 G/cm. The pulse sweep over a spatial region of 10 mm. The simulation accounts for a chemical-shift frequency offset of $\Omega_1/(2\pi) = 0.25$ kHz and $\Omega_1/(2\pi) = 0.75$ kHz. The red dashed line shows the analytical expression $4\gamma G/(R)(\Omega_1 + \Omega_2)z$.

7.3. Spatial encoding and J couplings

For weakly coupled spins, J couplings induce an oscillatory conversion between in-phase and anti-phase magnetisation. Consider for example an AX system of 2 homonuclear weakly coupled spins 1 and 2, free evolution of an initial term of the form $\sigma(0) = I_{1+}$ during a delay τ gives

$$\sigma_{\text{free}}(\tau) = (I_{1+}\cos(\pi J\tau) - 2iI_{1+}I_{2z}\sin(\pi J\tau)) \times \exp(-i\Omega_1\tau). \quad (65)$$

The application of a hard 180° pulse at a time $0 < t_\pi < \tau$ changes the sign of the coherence order and the chemical shift evolution, but has not influence on J modulation:

$$\sigma_\pi(\tau) = (I_{1-}\cos(\pi J\tau) + 2iI_{1-}I_{2z}\sin(\pi J\tau)) \times \exp(i\Omega_1(\tau - 2t_\pi)). \quad (66)$$

Similarly, J modulation takes place largely independently of spatial encoding in UF 2D NMR experiments, for weakly coupled spins. A small difference arises, however, because of the difference in flip time for the coupled spins. The density matrix after the application of two chirp pulses together with bipolar gradients is:

$$\sigma_{\text{UF}}(\tau) = (I_{1+}\cos(\pi J\tau') - 2iI_{1+}I_{2z}\sin(\pi J\tau')) \times \exp(-i4\frac{\gamma G}{R}\Omega_1 z), \quad (67)$$

where

$$\tau' = 2T_e - 2\frac{|\Omega_1 - \Omega_2|}{|R|}, \quad (68)$$

is the encoding time corrected for the difference in flip time between spins 1 and 2. J modulation effectively changes sign between the flip of spin 1 and that of spin 2.

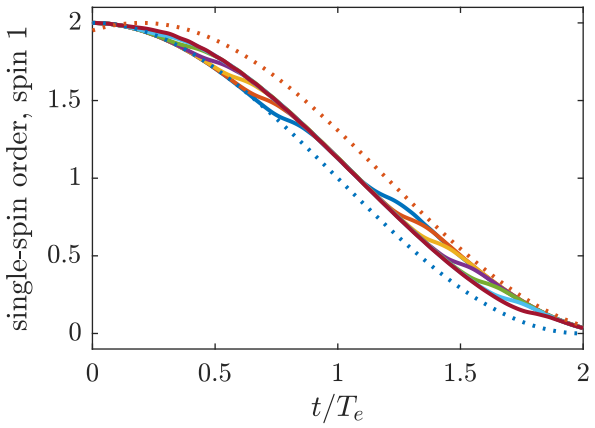

Figure 12: Trajectories of the spins for several slices, during a pair of frequency-swept pulses applied together with bipolar magnetic field gradient pulses, for a two-spin system. The initial state is $(1/\sqrt{2})I_{1+}$. The amount of single-spin order is shown for spin 1. The simulated pulse has an adiabaticity factor $Q = 6.28$ and a time-bandwidth product $TBW = 150$, and is applied together with a magnetic field gradient $G = RT_e/(\gamma L_s)$. The two spins have a chemical-shift frequency offset of $\pm RT_e/(20 \times 2\pi)$, and a mutual J coupling of $1/(4T_e)$. Trajectories are shown for 7 different slices, located at $i \times L_s/10$, for i ranging from 2 (blue) to 8 (dark red). Analytical J modulation curves $2\cos^2(\pi J t')$ are shown as dotted line, for $t' = t$ (blue) and for $t' = t - 2|\Omega_1 - \Omega_2|/|R|$ (orange).

Figure 12 shows a comparison between numerical simulations and analytical expressions for J modulation during spatial encoding for a pair of weakly coupled spins. In this case, to capture the J modulation process, the plotted quantity is

$$A_1(t) = \sum_{r\in\{5,9,13\}} |b_r|^2, \tag{69}$$

corresponding to single-spin terms for spin 1. It can be seen that J modulation is almost unaffected by spatial encoding, except for a small time shift. These results have been used to optimise the sensitivity of UF 2D NMR experiments by the judicious choice of the J modulation time [53, 54].

The expressions given here are useful for the analysis of systems of weakly coupled spins. For systems of strongly coupled spins, while numerical simulation do to some extent reproduce experimental findings [53], no analytical description of the spatial encoding process has been reported.

8. Discussion

Spatial parallelisation is now well-established as a powerful approach to accelerate multidimensional experiments. While they were originally reported independently, experiments for UF IR, UF 2D NMR, UF DOSY and UF LNMR can be described with a common theoretical and numerical framework, which may help to design new or improved experiments.

It has recently been shown that non-linear frequency sweeps can be used to perform more efficient spatial encoding. This was shown in the case of spatial encoding of relaxation, using a logarithmic frequency sweep [55]. With this sweep, the recovery delay varies exponentially with position, which makes it possible to measure broader ranges of relaxation rates than with linear sampling. Before this work, virtually all the experiments based on continuous spatial encoding used a linear frequency sweep. The use of non-linear spatial encoding could be generalised to other spatial encoding experiments. In the case of diffusion and relaxation, the associated change of the acquisition and processing stages are minimal, because implementations of the Laplace transform do not require a uniform sampling of the time or spatial frequency dimension. For UF 2D NMR, non-uniform spatial encoding would also require a significant change of the acquisition and processing stage, and the benefits would be less obvious.

Spatial parallelisation of a delay in a pulse sequence can also be used in cases where the parallelised dimension is not subsequently resolved [24]. The resulting spectrum is then a continuous sum over a range of delays. This is for example the case for the Z filter described by Thrippleton and Keeler, in which the chemical-shift evolution delay of zero-quantum coherences is parallelised, to suppress the signals from pathways that go through ZQ coherences [19]. This is also the case in PSYCHE experiments [20, 56], in which signals that originate from coherence transfer, in a stimulated echo with two small-tip-angle rotations, are suppressed by spatial parallelisation of chemical-shift encoding delays. Frequency-swept pulses could also be used to parallelise other delays, such as the build-up time of multi-spin terms in multiple-quantum NMR experiments.

Strategies for spatial encoding have also been reported, that rely on the simultaneous application of several frequency-swept pulses. For example, a simultaneous sweep of the two halves of the sample in opposite directions was used to improve lineshapes in UF 2D NMR [57]. Applying the sum of two frequency-swept pulses approximately yields the sum of the separate application of each pulse, when the pulses sweep over different spatial regions. Simultaneous small-tip angle sweeps are also used in the PSYCHE pulse sequence, although in this case these act on the same spatial region and the exact relationship to the single-sweep case remains to be characterised. Numerical simulation of the spin dynamics during PSYCHE decoupling have recently been reported [32].

The examples discussed in section 6 concern ideal cases, in which only the information of interest is included in the theoretical and analytical descriptions. The models can be expanded to account for other effects, such as the effect of diffusion or relaxation in UF 2D NMR experiments. It has, for example, been shown that the effect of diffusion in UF 2D NMR result in modest sensitivity losses and an improved lineshape [58, 59] Spatially encoded experiments are also sensitive to the effect of macroscopic sample motion such as convection and flow. This effect can be compensated to some extent in the case of diffusion encoding [45, 13]. In the case of chemical-shift encoding, no approach has yet been found, however, to preserve the spatially encoded information for a moving sample [60].

Frequency-swept pulses are a central ingredient of ultrafast spatially encoded NMR experiments. They are frequently used in the form of linearly-swept chirp pulse, that are well understood, and applied for applications ranging from reaction mon-

itoring to the characterisation of metabolic mixtures. Ongoing developments that involve more complex frequency-swept pulses, and combinations thereof, promise to expand the applicability and accuracy of UFNMR methods.

Acknowledgments

I would like to thank many colleagues for discussions on frequency-swept pulses, and in particular Rituraj Mishra, Corentin Jacquemmoz, Patrick Giraudeau, Mohammadali Foroozandeh, Philippe Pelupessy, and Ville-Veikko Telkki for discussions during the preparation of this manuscript.

This work has received funding from the European Research Council (ERC) under the European Union's Horizon 2020 research and innovation program (grant agreement no 801774), the Region Pays de la Loire (Connect Talent).

References

[1] M. Garwood, L. DelaBarre, The return of the frequency sweep: Designing adiabatic pulses for contemporary NMR, J. Magn. Reson. 153 (2001) 155–177.

[2] L. Frydman, T. Scherf, A. Lupulescu, The acquisition of multidimensional NMR spectra within a single scan, Proc. Natl. Acad. Sci. U. S. A. 99 (2002) 15858–15862.

[3] N. M. Loening, M. J. Thrippleton, J. Keeler, R. G. Griffin, Single-scan longitudinal relaxation measurements in high-resolution NMR spectroscopy, J. Magn. Reson. 164 (2003) 321–328.

[4] M. J. Thrippleton, N. M. Loening, J. Keeler, A fast method for the measurement of diffusion coefficients: One-dimensional DOSY, Magn. Reson. Chem. 41 (2003) 441–447.

[5] P. Pelupessy, Adiabatic single scan two-dimensional NMR spectrocopy, J. Am. Chem. Soc. 125 (2003) 12345–12350.

[6] Y. Shrot, B. Shapira, L. Frydman, Ultrafast 2D NMR spectroscopy using a continuous spatial encoding of the spin interactions, J. Magn. Reson. 171 (2004) 163–170.

[7] A. Tal, B. Shapira, L. Frydman, A continuous phase-modulated approach to spatial encoding in ultrafast 2D NMR spectroscopy, J. Magn. Reson. 176 (2005) 107–114.

[8] M. Gal, M. Mishkovsky, L. Frydman, Real-time monitoring of chemical transformations by ultrafast 2D NMR spectroscopy, J. Am. Chem. Soc. 128 (2006) 951–956.

[9] M. Gal, P. Schanda, B. Brutscher, L. Frydman, UltraSOFAST HMQC NMR and the repetitive acquisition of 2D protein spectra at Hz rates, J. Am. Chem. Soc. 129 (2007) 1372–1377.

[10] A. Herrera, E. Fernández-Valle, R. Martínez-Álvarez, D. Molero-Vílchez, Z. D. Pardo-Botero, E. Sáez-Barajas, Monitoring organic reactions by UF-NMR spectroscopy, Magn. Reson. Chem. 53 (2015) 952–970.

[11] P. E. Smith, K. J. Donovan, O. Szekely, M. Baias, L. Frydman, Ultrafast NMR T1 relaxation measurements: Probing molecular properties in real time, ChemPhysChem 14 (2013) 3138–3145.

[12] R. Boisseau, U. Bussy, P. Giraudeau, M. Boujtita, In situ ultrafast 2D NMR spectroelectrochemistry for real-time monitoring of redox reactions, Anal. Chem. 87 (2015) 372–375.

[13] G. Hamdoun, L. Guduff, C. Van Heijenoort, C. Bour, V. Gandon, J. N. Dumez, Spatially encoded diffusion-ordered NMR spectroscopy of reaction mixtures in organic solvents, Analyst 143 (2018) 3458–3464.

[14] P. Giraudeau, Y. Shrot, L. Frydman, Multiple ultrafast, broadband 2D NMR spectra of hyperpolarized natural products, J. Am. Chem. Soc. 131 (2009) 13902–13903.

[15] S. Ahola, V. V. Zhivonitko, O. Mankinen, G. Zhang, A. M. Kantola, H. Y. Chen, C. Hilty, I. V. Koptyug, V. V. Telkki, Ultrafast multidimensional Laplace NMR for a rapid and sensitive chemical analysis, Nat. Commun. 6 (2015) 1–7.

[16] L. Guduff, D. Kurzbach, C. van Heijenoort, D. Abergel, J. N. Dumez, Single-Scan13C Diffusion-Ordered NMR Spectroscopy of DNP-Hyperpolarised Substrates, Chem. - A Eur. J. 23 (2017) 16722–16727.

[17] P. Giraudeau, L. Frydman, Ultrafast 2D NMR: An Emerging Tool in Analytical Spectroscopy, Annu. Rev. Anal. Chem. 7 (2014) 129–161.

[18] T. Jézéquel, C. Deborde, M. Maucourt, V. Zhendre, A. Moing, P. Giraudeau, Absolute quantification of metabolites in tomato fruit extracts by fast 2D NMR, Metabolomics 11 (2015) 1231–1242.

[19] M. J. Thrippleton, J. Keeler, Elimination of zero-quantum interference in two-dimensional NMR spectra, Angew. Chemie - Int. Ed. 42 (2003) 3938–3941.

[20] M. Foroozandeh, R. W. Adams, N. J. Meharry, D. Jeannerat, M. Nilsson, G. A. Morris, Ultrahigh-resolution NMR spectroscopy, Angew. Chemie - Int. Ed. 53 (2014) 6990–6992.

[21] S. Ahola, V. V. Telkki, Ultrafast two-dimensional NMR relaxometry for investigating molecular processes in real time, ChemPhysChem 15 (2014) 1687–1692.

[22] J. G. Pipe, A fast method for obtaining a "continuous" sample of the inversion-recovery curve using spatially swept adiabatic inversion, J. Magn. Reson. 99 (1992) 582–589.

[23] Y. Shrot, L. Frydman, Single-scan 2D DOSY NMR spectroscopy, J. Magn. Reson. 195 (2008) 226–231.

[24] J. N. Dumez, Spatial encoding and spatial selection methods in high-resolution NMR spectroscopy, Prog. Nucl. Magn. Reson. Spectrosc. 109 (2018) 101–134.

[25] J. M. Bohlen, M. Rey, G. Bodenhausen, Refocusing with chirped pulses for broadband excitation without phase dispersion, J. Magn. Reson. 84 (1989) 191–197.

[26] E. Kupče, R. Freeman, Adiabatic Pulses for Wideband Inversion and Broadband Decoupling, J. Magn. Reson. Ser. A 115 (1995) 273–276.

[27] Y. Shrot, L. Frydman, Spatially encoded NMR and the acquisition of 2D magnetic resonance images within a single scan, J. Magn. Reson. 172 (2005) 179–190.

[28] G. Jeschke, S. Pribitzer, A. Doll, Coherence Transfer by Passage Pulses in Electron Paramagnetic Resonance Spectroscopy, J. Phys. Chem. B 119 (2015) 13570–13582.

[29] H. J. Hogben, M. Krzystyniak, G. T. P. Charnock, P. J. Hore, I. Kuprov, Spinach - A software library for simulation of spin dynamics in large spin systems, J. Magn. Reson. 208 (2011) 179–194.

[30] I. Kuprov, Fokker-Planck formalism in magnetic resonance simulations, J. Magn. Reson. 270 (2016) 124–135.

[31] L. Guduff, A. J. Allami, C. van Heijenoort, J.-N. Dumez, I. Kuprov, Efficient simulation of ultrafast magnetic resonance experiments, Phys. Chem. Chem. Phys. 19 (2017) 17577–17586.

[32] M. Foroozandeh, Spin Dynamics During Chirped Pulses: Applications to Homonuclear Decoupling and Broadband Excitation, J. Magn. Reson. (2020).

[33] A. Tal, L. Frydman, Single-scan multidimensional magnetic resonance, Prog. Nucl. Magn. Reson. Spectrosc. 57 (2010) 241–292.

[34] V. V. Telkki, V. V. Zhivonitko, Ultrafast NMR diffusion and relaxation studies, Annu. Reports NMR Spectrosc. 97 (2019) 83–119.

[35] M. Gal, L. Frydman, Ultrafast Multidimensional NMR: Principles and Practice of Single-Scan Methods, in: Encycl. Magn. Reson., volume 43, John Wiley & Sons, Ltd, Chichester, UK, 2008, pp. no–no. URL: `http://doi.wiley.com/10.1002/9780470034590.emrstm1024`. doi:`10.1002/9780470034590.emrstm1024`.

[36] J. Valette, F. Lethimonnier, V. Lebon, About the origins of NMR diffusion-weighting induced by frequency-swept pulses, J. Magn. Reson. 205 (2010) 255–259.

[37] D. Kunz, Use of frequency-modulated radiofrequency pulses in MR imaging experiments, Magn. Reson. Med. 3 (1986) 377–384.

[38] D. Kunz, Frequency-modulated radiofrequency pulses in spin-echo and stimulated-echo experiments, Magn. Reson. Med. 4 (1987) 129–136.

[39] M. H. Levitt, L. Di Bari, Steady state in magnetic resonance pulse experiments, Phys. Rev. Lett. 69 (1992) 3124–3127.

[40] B. Gouilleux, L. Rouger, P. Giraudeau, Ultrafast 2D NMR: Methods and Applications, Annu. Reports NMR Spectrosc. 93 (2018) 75–144.

[41] C. Wu, M. Zhao, S. Cai, Y. Lin, Z. Chen, Ultrafast 2D COSY with constant-time phase-modulated spatial encoding, J. Magn. Reson. 204 (2010) 82–90.

[42] P. Giraudeau, S. Akoka, Resolution and sensitivity aspects of ultrafast J-resolved 2D NMR spectra, J. Magn. Reson. 190 (2008) 339–345.

[43] E. O. Stejskal, J. E. Tanner, Spin diffusion measurements: Spin echoes in the presence of a time-dependent field gradient, J. Chem. Phys. 42 (1965)

288–292.
[44] Y. Shrot, L. Frydman, Spatial encoding strategies for ultrafast multidimensional nuclear magnetic resonance, J. Chem. Phys. 128 (2008) 1–14.
[45] L. Guduff, I. Kuprov, C. Van Heijenoort, J. N. Dumez, Spatially encoded 2D and 3D diffusion-ordered NMR spectroscopy, Chem. Commun. 53 (2017) 701–704.
[46] P. Callaghan, Principles of Nuclear Magnetic Resonance Microscopy, Clarendon Press, Oxford, 1993.
[47] N. M. Loening, J. Keeler, G. A. Morris, One-dimensional DOSY, J. Magn. Reson. 153 (2001) 103–112.
[48] S. Ahola, O. Mankinen, V. V. Telkki, Ultrafast NMR diffusion measurements exploiting chirp spin echoes, Magn. Reson. Chem. 55 (2017) 341–347.
[49] P. Pelupessy, E. Rennella, G. Bodenhausen, High-Resolution NMR in Magnetic Fields with Unknown Spatiotemporal Variations, Science (80-.). 324 (2009) 1693–1697.
[50] Y. Lin, Z. Zhang, S. Cai, Z. Chen, High-resolution 2D J -resolved spectroscopy in inhomogeneous fields with two scans, J. Am. Chem. Soc. 133 (2011) 7632–7635.
[51] A. L. Guennec, P. Giraudeau, S. Caldarelli, J. N. Dumez, Ultrafast double-quantum NMR spectroscopy, Chem. Commun. 51 (2015) 354–357.
[52] M. G. Concilio, C. Jacquemmoz, D. Boyarskaya, G. Masson, J. N. Dumez, Ultrafast Maximum-Quantum NMR Spectroscopy for the Analysis of Aromatic Mixtures, ChemPhysChem (2018) 3310–3317.
[53] B. Gouilleux, L. Rouger, B. Charrier, I. Kuprov, S. Akoka, J.-N. Dumez, P. Giraudeau, Understanding J-Modulation during Spatial Encoding for Sensitivity-Optimized Ultrafast NMR Spectroscopy, ChemPhysChem 16 (2015) 3093–3100.
[54] L. Rouger, B. Gouilleux, M. Pourchet-Gellez, J. N. Dumez, P. Giraudeau, Ultrafast double-quantum NMR spectroscopy with optimized sensitivity for the analysis of mixtures, Analyst 141 (2016) 1686–1692.
[55] V. V. Zhivonitko, M. S. Ullah, V. V. Telkki, Nonlinear sampling in ultrafast Laplace NMR, J. Magn. Reson. 307 (2019) 106571.
[56] M. Foroozandeh, G. A. Morris, M. Nilsson, PSYCHE Pure Shift NMR Spectroscopy, Chem. - A Eur. J. (2018) doi: 10.1002/chem.201800524.
[57] B. Shapira, Y. Shrot, L. Frydman, Symmetric spatial encoding in ultrafast 2D NMR spectroscopy, J. Magn. Reson. 178 (2006) 33–41.
[58] Y. Shrot, L. Frydman, The effects of molecular diffusion in ultrafast two-dimensional nuclear magnetic resonance, J. Chem. Phys. 128 (2008) 1–15.
[59] P. Giraudeau, S. Akoka, Sensitivity losses and line shape modifications due to molecular diffusion in continuous encoding ultrafast 2D NMR experiments, J. Magn. Reson. 195 (2008) 9–16.
[60] C. Jacquemmoz, F. Giraud, J. N. Dumez, Online reaction monitoring by single-scan 2D NMR under flow conditions, Analyst 145 (2020) 478–485.